doi:10.3788/gzxb20174611.1125003

高速低能耗垂直腔面发射激光器的基于氧化限制孔径影响的强度噪声分析

李惠,贾晓卫,魏泽坤
(青岛科技大学 数理学院,山东 青岛 266062)

摘 要:对不同氧化孔径尺寸的高速,低能耗的垂直腔面发射激光器(VCSEL)进行了相对强度噪声(RIN)分析.小氧化物尺寸孔径的VCSELs器件更适用于低能耗数据传输,且RIN特性与低能耗性能没有冲突.实验结果表明,适合低能耗、高温度稳定性工作的小氧化孔径VCSELs器件同时表现出较好的噪声性能.高速低能耗VCSEL能够满足32GFC光纤通道标准的RIN要求,在将来的高性能计算机应用中具有巨大优势.

关键词:噪声;垂直腔面发射激光器(VCSEL);高速;低能耗;光互连
中图分类号:TN 249 **文献标识码**:A **文章编号**:1004-4213(2017)11-1125003-8

Oxide-Aperture Dependent-RIN Research of High-speed, Energy-Efficient 980 nm VCSELs

LI Hui, JIA XIAO-wei, WEI Ze-kun
(*College of Mathematical and Physical Sciences, Qingdao University of Science and Technology, Qingdao, Shandong* 266061, *China*)

Abstract: Oxide-aperature-diameter dependent analysis of RIN for high-speed, energy-efficient Vertical-Cavity Surface Emitting Lasers (VCSELs) have been performed. Small oxide-aperture diameter VCSELs are prefered for low energy consumption data transmission. We demonstrate that energy efficiency is not in conflict with our VCSELs′ RIN characteristics. The experimental results indicate that small oxide-aperture diameter VCSELs, which are the most suitable for energy-efficient, temperature-stable operation, exhibit lower laser RIN due to less mode competition inside the smaller optical cavity volume. Our energy-efficient VCSELs fulfill the RIN requirements of the 32G Fibre Channel standard. These devices are advantageous for future high performance computer applications.

Key words: RIN; Vertical-Cavity Surface-Emitting Lasers (VCSEL); High-speed; Energy-effcient; Optical interconnect
OCIS Codes: 250.7260; 250.7270; 140.7260

0 Introduction

Vertical Cavity Surface Emitting Lasers (VCSELs) are a key enabling technology for both deployed and future short-reach Optical Interconnects (OIs). The attributes of VCSEL-based OIs include low energy consumption, low cost, efficient optical coupling, and direct current modulation[1-4]. In modern data

Foundation item: The National Natural Science Foundation of China (No. 11647169), the Natural Science Foundation of Shandong Province (No. ZR2016FB05), the Natural Science Foundation of Qingdao (No. 16-5-1-8-jch), and the Open Fund of the State Key Laboratory of Luminescence and Applications.
First author: LI Hui (1986—), female, Ph.D. degree, lecturer, mainly focuses on high-speed semiconductor laser. Email: lilinlu88@163.com
Received: Jun.9, 2017; **Accepted**: Jul.17, 2017

centers it is common to find that about 90% of the optical interconnects within and between servers, whether passive or active optical cables, are 100 m or shorter with the most often deployed length in the range of 20-30 m. The typical lengths of the short-reach optical interconnects is not expected to drastically change as the bit rate migrates to 25-28 Gbit/s. New opportunities in short-reach optical interconnects at distances of ~20 m or less are emerging as the energy efficiency and the bandwidth density of complete optical links surpass the energy efficiency and the bandwidth density of electrical interconnects. High speed and energy efficiency of OIs is achieved by directly modulating small oxide-aperture diameter VCSELs biased at moderate currents with simple Non-Return-to-Zero (NRZ) on-off keying data coding[5-6]. This modulation format is limited by the analog −3-dB bandwidths of the VCSELs. The VCSEL′ Relative Intensity Noise (RIN), which is a major source of OI system noise, degrades the signal quality and increases the Bit Error Rate (BER) under certain conditions[7]. A low RIN floor across the operating range is needed to achieve a large signal-to-noise ratio (SNR). RIN characteristics often get less attention in device research, where the focus is on the modulation characteristics. System limitations due to poor RIN often are compensated by over-driving the VCSELs, getting larger modulation bandwidth than needed as compared to a system with better RIN characteristics[8]. This strategy increases strongly the required operating power and is in contrast to efficiency optimized approaches.

For applications in short-reach optical interconnects we see a massive opportunity to further develop our energy-efficient VCSELs but for emission at ~980 nm due to the inherent higher temperature stable performance of the 980 nm VCSELs. However in addition to energy efficiency and bit rate we are also very interested in optimizing other VCSEL attributes including the temperature stability, and eventually the reliability and manufacturability as well. For a given set of attributes or specifications the optimal VCSEL emission wavelength may be slightly different than it would be for solely an optimal energy-efficient device at a reasonable high bit rate. The point is that the energy-efficiency of the VCSEL may no longer be ignored as a small fraction of the overall link power[9], and this is especially true for high density, high bandwidth VCSELs that will be integrated as individual devices or as arrays with silicon, flexible plastic materials, fabrics, or a cornucopia of other host materials. For these reasons we seek to optimize the energy efficiency, bit rate, modal properties, and other attributes of 980 nm VCSELs, both individually and simultaneously.

980 nm GaAs-based VCSELs were designed, modeled, fabricated, and characterized. The RIN spectra of energy-efficient, temperature-stable 980-nm VCSELs were studied at different bias currents at room temperature for different oxide-aperture diameters. Low RIN operation is achieved even at low bias currents as required specifically for energy-efficient, error-free data transmission operation.

1 980 NM VCSEL DESIGN

The VCSELs are grown on 76.2 mm-diameter {001}-oriented 2-degree off n-doped GaAs wafers by the commercial foundry IQE plc Cardiff, UK by metal-organic chemical-vapor deposition (MOCVD) as we previously reported. We employ five ~4.2 nm-thick compressively strained $In_{0.21}Ga_{0.79}As$ quantum wells (QWs) and ~6.0 nm-thick $GaAs_{0.12}P_{0.88}$ partially strain compensating barrier layers to form the active region within a 1.0λ-thick microcavity. GaAs barrier layers are commonly used to surround the compressively strained InGaAs QWs for the active region of GaAs-based 980-nm VCSELs. GaAsP is another candidate barrier material, where the GaAsP layers are in tensile strain and serve to partially counter the compressive QW strain. $GaAs_{0.88}P_{0.12}$ barrier layers with 0.43% tensile strain and no-strain GaAs barrier layers are choose to surround the $In_{0.21}Ga_{0.79}As$ QWs. The QW thickness is chosen to be 4.2 nm, the barrier thickness is 6 nm, and thus the combined single $GaAs_{0.88}P_{0.12}/In_{0.21}Ga_{0.79}As/GaAs_{0.88}P_{0.12}$ QW structure lattice-matched to GaAs is below the critical layer thickness limit. The band alignment of $In_{0.21}Ga_{0.79}As/GaAs_{0.88}P_{0.12}$ and $In_{0.21}Ga_{0.79}As/GaAs$ QWs are calculated using the model-solid theory. The use of GaAsP barrier layers results in a better band alignment of the strain-compensated QWs compared to standard $In_{0.21}Ga_{0.79}As/GaAs$ QWs. For $In_{0.21}Ga_{0.79}As/GaAs$ the conduction band offset is 0.15 eV. The conduction band offset of $In_{0.21}Ga_{0.79}As/GaAs_{0.12}P_{0.88}$ QWs is 0.18 eV, 20% larger than the $In_{0.21}Ga_{0.79}As/GaAs$ QWs. An increased conduction band offset and valence band offset is beneficial for the

electron and hole confinement and also can reduce the thermal escape of carriers. VCSELs with strain compensated $In_{0.21}Ga_{0.79}As/GaAs_{0.88}P_{0.12}$ QWs will have less temperature sensitivity, enabling the VCSELs to have a better performance at high temperature, which has been proven by experimental comparison. The valence subbands are calculated using the k · p theory. $In_{0.21}Ga_{0.79}As/GaAs_{0.88}P_{0.12}$ QWs have a larger energy separation at the Γ point than the standard $In_{0.21}Ga_{0.79}As/GaAs$ QWs, between the first heavy hole HH1 and the first light hole LH1 subband. Also the in-plane effective mass of the holes become lighter. The carrier filling is mainly related to the in-plane effective mass of the holes, and thus the density of states in the valence and conduction bands are more closely matched, the population inversion is earlier achieved at lower injection carrier density, resulting in a higher differential gain and lower transparency carrier density.

Also, a −15 nm room temperature QW peak luminescence wavelength to etalon wavelength offset is employed to improve our VCSEL′ high temperature static and dynamic performance. The QW gain-to-etalon wavelength offset not only has an important influence on the static performance, but also a large impact on the high-speed modulation properties, as the change of the differential QW gain for a temperature increase is noticeably reduced. This effect can be predicted based on temperature dependent calculations of the differential gain. The differential gain versus wavelength at the threshold-gain-point for different temperatures is calculated by: 1) determining the threshold gain of the VCSELs at a given temperature accounting for mirror losses and absorption; 2) using the same approach to determine the parameters for the specific required QW gain; and 3) calculating the differential gain at this threshold-gain-point. The threshold gain is calculated to be here 472 cm^{-1} at 300 K. As expected, the calculations show that the differential gain peak moves to longer wavelengths with elevated temperatures and at the same time, the maximum gain decreases slowly, as shown in Fig. 1. An active region with high differential gain is desired for high bit rate VCSELs. A higher differential gain leads to a larger *D*-factor and thus a faster increase of relaxation resonance frequency with current. This enables the VCSEL to reach a larger modulation bandwidth before it is limited by damping or thermal effects. In order to illustrate the importance of the change in differential gain with temperature to the temperature stability of the devices, the results for gain-to-etalon wavelength offsets of 0, −5, −10, −15, −20 and −25 nm are depicted in Fig. 1. The highest differential gain is obtained when the gain-to-etalon wavelength offsets is 0 nm and the active region temperature is 300 K, and the differential gain decreases rapidly with increasing temperature. The temperature of the active region is always higher than the ambient temperature, thus a large differential gain at elevated temperatures is clearly important for a temperature robust VCSEL. The −15 nm gain-to-etalon wavelength offset design has a smoother change of the differential gain across the temperature range of 25-85 ℃ compared to offsets of 0 nm and −25 nm. The −15 nm offset also results in higher differential gain at temperatures above ~350 K as compared to a VCSEL with a 0 nm gain-to-etalon wavelength offset. This is clearly beneficial for operation at high bit rate at high temperatures for temperature stability. Also, this larger differential gain results in a large *D*-factor, which is an important factor for VCSELs reach a certain bandwidth at a low bias current, to enable a low operating power consumption. A larger offset, for example −25 nm, results in a lower differential gain at 300-340 K. In addition, the differential gain at from ~360-385 K is less than what is possible with a −15 nm offset.

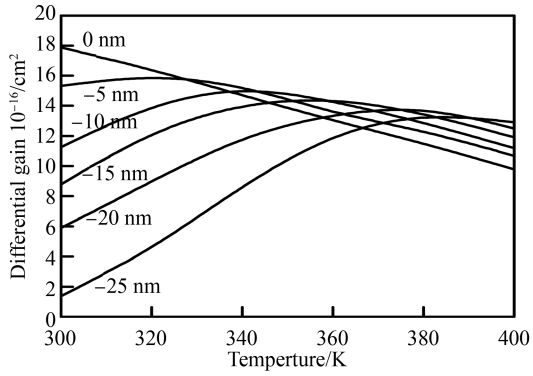

Fig.1 Calculated differential gain versus temperature for 300 K gain-to-etalon wavelength offsets of 0, −5, −10, −15, −20, and −25 nm

Doped $Al_{0.12}Ga_{0.88}As/Al_{0.90}Ga_{0.10}As$ Distributed Bragg Reflectors (DBRs) with ~20 nm-thick linear graded interfaces with 24 and 37.5 periods were used for the top and bottom mirror, respectively. As shown schematically in Figure 2, The VCSELs were processed into a high-speed Ground-Signal-Ground

(GSG) pad layout configuration to facilitate high bit rate data transmission testing. Two dry-etched mesas were used to facilitate improved heat dissipation. The top mesa diameter varies from about 18 μm to 31 μm in steps of initially 0.5 μm and then 1.0 μm resulting in a column of 16 VCSELs with different oxide aperture diameters after the simultaneous selective oxidation of all VCSELs on a given wafer piece. A given bottom mesa diameter is 30 μm larger than its top mesa diameter. The n-type bottom contact is processed into the shape of a three-quarter ring. Thick (~8 μm) dry-etched bisbenzo-cyclobutene (BCB) is used to reduce electrical parasitics, approximately planarize the surface, and enable the evaporation of the coplanar contact pads for on-wafer high frequency probing. The device pitch and contact sizes were designed to facilitate fast automatic Continuous Wave (CW) wafer-level automated characterization. In Figure 3 we show the real refractive index profile of our 980 nm VCSELs in and around the QW active region and optical cavity, along with the electric-field intensity on resonance.

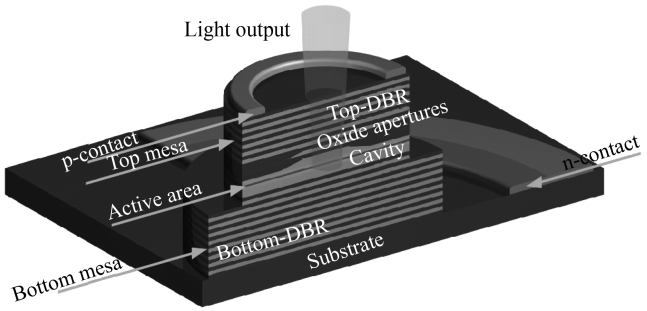

Fig.2 Simplified schematic diagram (not to scale) of the fabricated 980 nm VCSEL

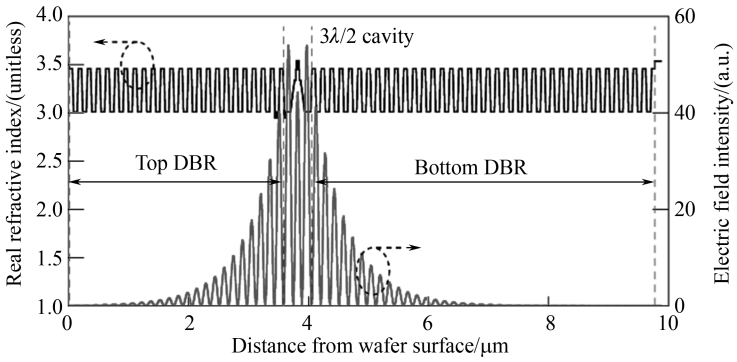

Fig.3 Real refractive index and electric-field intensity both versus distance from the top surface for the 980 nm VCSEL

2 Theory

Systematic investigations of 980 nm VCSELs wer performed in data transmission experiments focusing on energy efficiency. The results show that energy efficiency strongly depends on the oxide-aperture diameter. The smallest possible heat-to-bit-rate ratio is usually achieved by using small oxide-aperture diameter VCSELs biased at low currents. Since RIN is also strongly dependent on the oxide-aperture diameter and bias current, the RIN characteristics for energy-efficient VCSELs are important for overall OI system performance. The VCSEL′ Relative Intensity Noise (RIN), which is a major source of OI system noise, degrades the signal quality and increases the Bit Error Ratio (BER) under certain conditions. A low RIN floor across the operating range is needed to achieve a large Signal-to-Noise Ratio (SNR). RIN characteristics often get less attention in device research, where the focus is on the modulation characteristics. System limitations due to poor RIN are often compensated by over-driving the VCSELs, getting larger modulation bandwidth than needed as compared to a system with better RIN characteristics. This strategy increases strongly the required operating power and is in contrast to efficiency optimized approaches. Intensity noise in a laser diode is caused by random carrier and photon recombination and generation events, producing instantaneous time variations in the carrier and photon densities. The intensity noise mainly comes from the laser diode mode competition, as well as the optical interference between the coherent laser modes and the spontaneous light emission. A laser with low RIN is essential in

the pursuit of high fidelity optical transmission. According to Ref.[10], the RIN needs to be below −128 dB/Hz in 28 Gb/s data transmission. As RIN change with bias current and oxide-aperture diameter of VCSELs, it is useful to know the RIN value at the bias conditions for high bit rate and energy efficient operation.

The variation in photon density causes a variationin output power. The intensity noise (optical power fluctuations) is quantified using the relative intensity noise, which is the power noise normalized to the average power level. Optical power is detected with a fast photodetector, and thus the optical power fluctuations are transformed into electrical power fluctuations, which are measured with an Electrical Spectrum Analyzer (ESA). RIN can be expressed through the electrical values[11]

$$\mathrm{RIN}=\frac{N_{\mathrm{total}}}{P_{\mathrm{avg,elec}}}=\frac{N_{\mathrm{laser}}+N_{\mathrm{th}}+N_{\mathrm{PD,shot}}}{P_{\mathrm{avg,elec}}}(\mathrm{dB/Hz}) \tag{1}$$

where N_{total}(dBm/Hz) is the overall noise and $P_{\mathrm{avg,elec}}$ is the average electrical power. The overall noise N_{total} has three noise components: the VCSEL noise N_{laser}, the thermal noise N_{th}, and shot noise $N_{\mathrm{PD,shot}}$. The total amplified system noise power spectrum N_{total} is measure by the ESA with the laser diode on. By turning off the laser and keeping the operation of the photodetector and amplifiers, the signal analyzer measures only the thermal noise power spectrum $N_{\mathrm{th}}(f)$. N_{total} and N_{th} are weighted using the power spectral density per unit bandwidth with the unit of dBm/Hz, which can be calculated from noise power (dBm) and the resolution bandwidth (RBW) of the ESA using 1 dBm/Hz=1 dBm − 10log (BW). $G(f)$ (dB) is the frequency-depended amplifier power gain. Shot noise $N_{\mathrm{PD,shot}}=2qI_{\mathrm{ph}}R_{\mathrm{L}}$ is the shot noise power of the photodetector under the average input laser power P_0, I_{ph} is the photocurrent out of the photodetector, R_{L} is the load resistance of the amplifier input port. $N_{\mathrm{PD,shot}}$ appears at the photodetector and rises proportionally to the detected optical power. The average electrical power $P_{\mathrm{avg,\ elec}}=I_{\mathrm{ph}}^2R_{\mathrm{L}}$. After subtracting the system thermal noise and the photodetector shot noise, the intrinsic laser RIN can be extracted as

$$\mathrm{RIN}\,|_{\mathrm{laser}}(f)=\frac{[N_{\mathrm{total}}(f)-N_{\mathrm{th}}(f)]/G(f)-N_{\mathrm{PD,shot}}}{P_{\mathrm{avg,elec}}} \tag{2}$$

RIN corresponding to short noise can be calculated as

$$\mathrm{RIN}\,|_{\mathrm{PD,short}}=\frac{N_{\mathrm{PD,shot}}}{P_{\mathrm{avg,elec}}}=\frac{2qI_{\mathrm{ph}}R_{\mathrm{L}}}{I_{\mathrm{ph}}^2R_{\mathrm{L}}}=\frac{2q}{I_{\mathrm{ph}}} \tag{3}$$

For the laser diode RIN characterization, the VCSEL under test is biased at constant DC currents, and the output light is directly coupled into a 5 m-length lensed multimode fiber. The optical fiber is connected to a high speed New Focus 25 GHz photodetector 1 434-50, and the signal is amplified by two cascaded amplifiers SHF 100AP and SHF 804EA with gain of 19 and 20 dB to produce enough amplification to raise the signal above the noise floor of our spectrum analyzer. The frequency-depended total amplifier power gain $G(f)$ of two cascaded amplifiers is measured using a Network Analyzer. This factor $G(f)$ is subtracted from the noise measured by the ESA to compensate for the gain and the frequency response of the amplifiers. The New Focus photodetector has a build in bias monitor to measure the average photocurrent during the measurements. The average DC photocurrent can be calculated using a gain factor of 1 mV/μA to determine the average optical power. To measure one RIN value at a specific diode current, the first measurement is performed with the VCSEL turned on to determine the amplified overall noise N_{total} by using a Hewlett-Packard (HP) 8562A Spectrum Analyzer. Then a second measurement is performed with the VCSEL turned off, while leaving unchanged the photodetector and amplifiers, to determine the thermal noise N_{th}. The thermal noise does not depend on the optical power, which can be simply subtracted from the total noise. The resolution bandwidth of the ESA should be set low enough for the highest possible measurement precision with still enough sensitivity. The measurement precision is set at 30 kHz for following measurements.

3 Results

Laser diode RIN depends on many device performance and measurement test condition parameters, the most important are test frequency, laser diode output power, the operating temperature, modulation

frequency, modulation signal time delay, the magnitude of any optical feedback, the side-mode-suppression ratio of the emission spectra, and the relaxation oscillation frequency. Fig. 4(a) shows the measured RIN spectra for different bias currents above threshold current at room temperature for a ~5 to ~7 μm oxide-aperture diameter 980-nm VCSEL as well as the calculated shot noise level for the highest bias current. The behavior is as expected, with maximum noise intensity at the relaxation oscillation frequency, an increasing relaxation frequency with bias current, and a decrease in the RIN with an increase in bias current. This is because the predominant source of RIN is usually spontaneous emission. Hence, RIN reaches a maximum just above threshold when the spontaneous emission is typically at a maximum, and then the RIN decrease with increasing bias current, when the noise power do not increase too much while the optical power increased fast at high currents. These high-frequency RIN spectra contain well-defined peaks and reach the maximum RIN value at the relaxation oscillation frequency. For small oxide-aperture diameter (~5 μm) VCSEL, the noise saturates at the shot noise floor, but the noise of the large oxide-aperture diameter (~7 μm) VCSEL is higher due to mode competition. Due to much larger photocurrent, the shot noise level is also lower for larger oxide-aperture diameter VCSELs. Also, larger oxide-aperture diameter VCSELs are faster (small percentage of rollover current) to achieve low RIN than small ones even with higher order mode competition, where maximum RIN values and the output power versus current are shown. For the same low RIN value of −141 dB/Hz, the bias current need to be larger than 3 and 6.1 mA for ~3 and ~7 μm oxide-aperture diameter VCSELs, respectively. The rollover currents are 6 and 16 mA for ~3 and ~7 μm oxide-aperture diameter VCSELs. Bias current need to larger than 49% of the rollover current to have low RIN of −141 dB/Hz with ~3 μm oxide-aperture diameter VCSELs, but only 37.6% of the rollover current to have low RIN of −141 dB/Hz by using ~7 μm oxide-aperture diameter VCSELs. So larger oxide-aperture diameter VCSELs are faster to reach low RIN value, leading into lower RIN for high-bit rate operation.

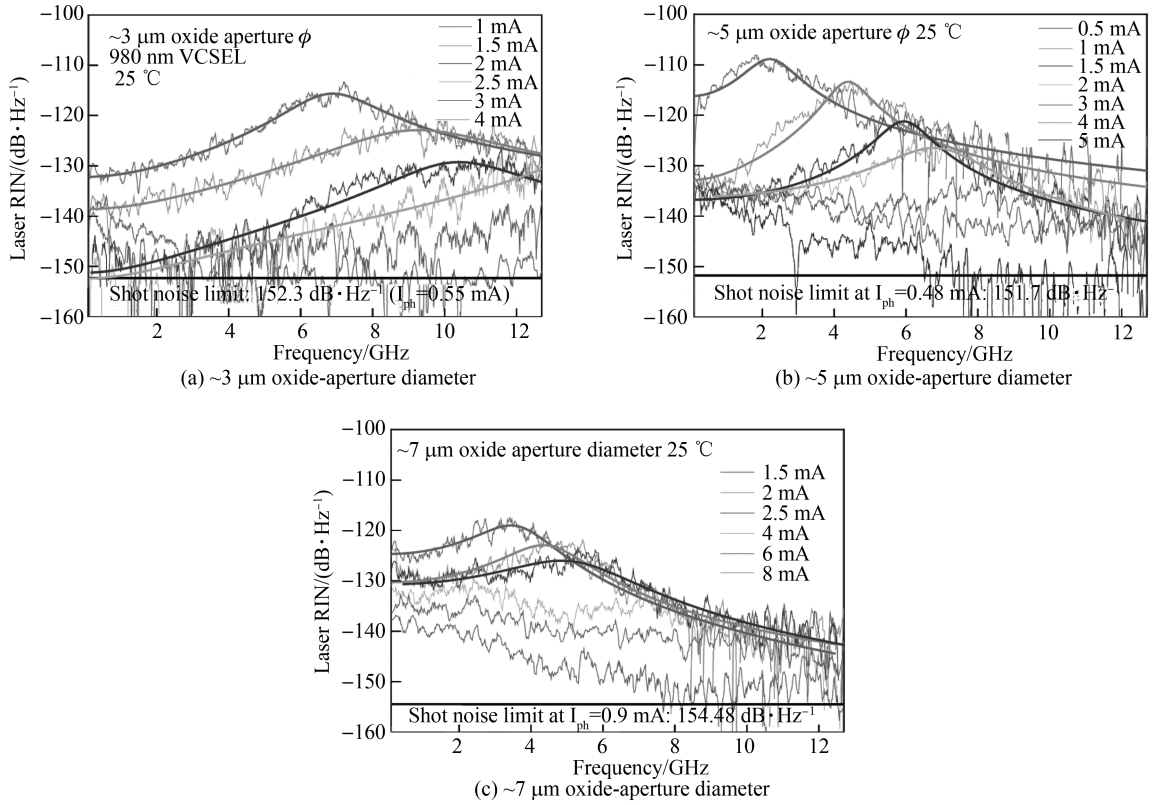

Fig.4 RIN spectra for different bias conditions at room temperature 980-nm VCSELs

The maximum value of laser diode RIN is at the relaxation resonance frequency. Fig. 5 shows these maximum RIN values versus bias current for VCSELs with ~3, 4, 5, 6 and 7 μm oxide-aperture diameters. The −3 dB bandwidth is extracted from the S21 measurements may be used to estimate the maximum achievable non-return-to-zero error-free bit rate that is possible with the given VCSEL when the

VCSEL is tested in the laboratory. It is clear that for a given constant current larger oxide-aperture diameters VCSELs have higher RIN values than smaller aperture ones. This is because the photon density is higher for smaller oxide-aperture diameter VCSELs due to the smaller optical mode volume. The relaxation resonance frequency and the damping both increase with an increase in photon density, which leads to lower RIN values for smaller oxide-aperture diameter VCSELs. At the same time, smaller oxide-aperture diameter VCSELs need smaller currents to achieve the same bandwidth, as show in Fig. 4. Small currents lead to a high RIN value. To achieve a high −3 dB bandwidth of 18.9 GHz, the RIN is only −141 and −151 dB/Hz for ~3 and ~4 μm oxide-aperture diameter VCSELs, and reaches the quantum limit for larger VCSELs. So small oxide-aperture diameter VCSELs not only benefit from a higher −3 dB bandwidth and lower power dissipation[12-13], but they also have sufficiently low noise, that enables the use of these VCSELs in future high-speed and low noise optical links with low energy consumption.

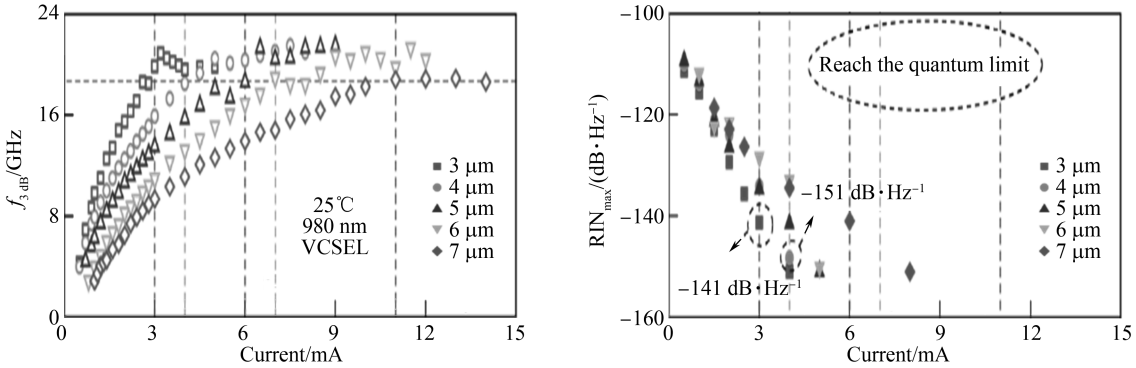

Fig.5 Comparison of maximum RIN value for 980-nm VCSELs with different oxide-aperture diameters operated at room temperature, and the −3 dB bandwidth vs. bias current

4 Conclusion

In conclusion, the RIN spectra of energy-efficient, temperature-stable 980-nm VCSELs were studied at different bias currents at room temperature for different oxide-aperture diameters. Low RIN operation is achieved even at low bias currents as required specifically for energy-efficient, error-free data transmission operation. The results show that smaller oxide-aperture diameter VCSELs exhibit lower laser diode RIN due to less mode competition at a given −3 dB bandwidth. The trend is consistent with energy-efficient operation. The VCSELs satisfy the bandwidth and RIN requirements for the 32 GFC Fibre Channel standard. Our small oxide-aperture diameter (3 to 4 μm) VCSELs not only benefit from a larger −3 dB bandwidth and lower energy dissipation per transmitted bit, but they also show extremely low noise. being advantageous for short reach optical interconnects in high performance computers and in board-to-board and chip-to-chip integrated photonics systems.

References

[1] LARSSON A. Advances in VCSELs for communication and sensing[J]. *IEEE Journal of Selected Topics in Quantum Electronics*, 2011, **17**(6): 1552-1567.

[2] KASUKAWA A. VCSEL technology for green optical interconnects[J]. *IEEE Photonics Journal*, 2012, **4**(2): 642-646.

[3] BIMBERG D, LARSSON A, JOEL A. Faster, more frugal, greener VCSELs[J]. *Compound Semiconductor*, 2014: 22.

[4] LIU Li-jie, WU Yuan-da, WANG Yue, *et al*. Research progress of 1310 nm VCSELs chip technology[J]. *Chinese Journal of Luminescence*, 2016, **37**(7): 809-815.

[5] MOSER P, WOLF P, LARISCH G, *et al*. Energy-efficient oxide-confined high-speed VCSELs for optical interconnects [C]. SPIE, 2014: 9001103.

[6] LI Hui, WOLF P, MOSER P, *et al*. Energy-efficient and temperature-stable 980 nm VCSELs for 35 Gb/s error-free data transmission at 85 ℃ with 139 fJ/bit dissipated heat[J]. *IEEE Photonics Technology Letters*, 2014, **26**(23): 2349-2352.

[7] TAN F, WU F, LIU M, *et al*. 850 nm oxide VCSEL with low relative intensity noise and 40 Gb/s error free data transmission[J]. *IEEE Photonics Technology Letters*, **26**(3): 289-292.

[8] TSAI C, CHANG S, PONG C, *et al*. RIN suppressed multimode 850-nm VCSEL for 56-Gbps 16-QAM OFDM and 22-Gbps PAM-4 transmission[C]. Optical Fiber Communication Conference Optical Society of America, 2016: Th4D. 2.

[9] MILLER D, Device requirements for optical interconnects to silicon chips[J]. *Proceedings of the IEEE*, 2009, **97**: 1166-1185.

[10] Fibre Channel Roadmaps v1.8[P]. http://fibrechannel.org/fibre-channel-roadmaps.html

[11] TAN F, WU M, LIU M, *et al*. Relative intensity noise in high speed microcavity laser[J]. *Applied Physics Letters*, 2013, **103**(14): 141116.

[12] LI Hui, WOLF P, MOSER P, *et al*. Energy-efficient and temperature-stable 980 nm VCSELs for 35 Gb/s error-free data transmission at 85 ℃ with 139 fJ/bit Dissipated Heat[J]. *IEEE Photonics Technology Letters*, **26**(23): 2349-2352.

[13] CAI Li-e, ZHANG Bao-ping, ZHANG Jiang-yong, *et al*. Fabrication and characteristics of GaN-based blue VCSEL[J]. *Chinese Journal of Luminescence*, 2016, **37**(4): 452-456.